Improved Electron Transport Properties of Zn-rich In-Ga-Zn-O Thin Film Transistors

Prashant Ghediya[1,*#], Hui Yang[1,2#], Takashi Fujimoto[3], Yuqiao Zhang[4,5], Yasutaka Matsuo[1], Yusaku Magari[1], and Hiromichi Ohta[1,*]

[1] *Research Institute for Electronic Science, Hokkaido University, N20W10, Kita, Sapporo 001-0020, Japan*

[2] *Institute of Optoelectronic Technology, Beijing Jiaotong University, Beijing 100044, China*

[3] *Graduate School of Information Science and Technology, Hokkaido University, Sapporo 060-0814, Japan*

[4] *Institute of Quantum and Sustainable Technology (IQST), School of Chemistry and Chemical Engineering, Jiangsu University, Zhenjiang 212013, China*

[5] *Foshan (Southern China) Institute for New Materials, Foshan 528200, China*

[#] Contributed equally to this work

*Email: prashantghediya@gmail.com, hiromichi.ohta@es.hokudai.ac.jp

KEYWORDS: $InGaO_3(ZnO)_m$, field effect mobility, effective mass, thermopower modulation, effective channel thickness

Abstract: Amorphous transparent oxide semiconductor $InGaZnO_4$-based thin film transistors (TFTs) have been practically used as the backplane of flat panel displays. For future higher-definition displays, alternative active materials with a higher field effect mobility (μ_{FE}) are necessary. Although there are a few reports on $InGaO_3(ZnO)_m$ with Zn-rich composition ($IGZO_m$)-based TFTs, their electron transport properties have not been clarified. Here, we show that a Zn-rich composition enhances the electron transport properties of $IGZO_m$-TFTs. The best TFT performance was obtained for $m = 7$ (μ_{FE} ~12 $cm^2\ V^{-1}\ s^{-1}$, subthreshold swing ~0.1 V $decade^{-1}$, and a negligibly small bias stress shift). The carrier effective mass (m^*) of $IGZO_m$ films was found to be 0.16 m_0, independent of the m-value. We found that μ_{FE} of $IGZO_m$-TFT increased with the m-value for $m \leq 7$, whereas it decreased for $m > 7$ due to the crystallization. The thermopower modulation analyses revealed that the effective channel thickness increased with m ($m \leq 7$) which resulted in a longer carrier relaxation time. The present results provide an improving strategy toward new material design for next-generation TFTs with higher μ_{FE} values.

Introduction

Amorphous transparent oxide semiconductor $InGaZnO_4$ (a-IGZO)-based thin film transistors (TFTs) are widely applied as the backplane of flat panel displays.[1, 2] In 2004, Nomura and Hosono *et al*.[3] demonstrated that a-IGZO-TFTs exhibit excellent transistor characteristics with a rather high field effect mobility (μ_{FE} ~7 $cm^2\ V^{-1}\ s^{-1}$). The reported value is an order of magnitude higher than that of a-Si (~0.5 $cm^2\ V^{-1}\ s^{-1}$). Since then, several display companies have vigorously developed and commercialized large-sized liquid crystal displays (LCDs) and organic light emitting diode displays (OLEDs) using

a-IGZO-TFTs as the backplane. Although a-IGZO-TFTs are widely applied nowadays, μ_{FE} must be increased for higher-definition pixeled and wearable displays. Therefore, alternative active materials with a higher μ_{FE} are still demanded.

In this study, we focus on $InGaO_3(ZnO)_m$ with higher m-values ($IGZO_m$ hereafter) as a potential alternative active material. $IGZO_m$ crystallizes with a layered structure composed of an InO_2^- layer and a $GaO(ZnO)_m^+$ block, which are alternately stacked along the c-axis.[4] Since there is a thermodynamically stable crystalline phase, ceramic targets of $IGZO_m$ can easily be fabricated, good for practical applications that require very large-sized crack-free ceramic targets. Nomura *et al*.[5] fabricated TFTs in $InGaO_3(ZnO)_5$ single crystal films using reactive solid-phase epitaxy.[6] Their TFTs exhibited high mobility μ_{FE} ~80 $cm^2\ V^{-1}\ s^{-1}$, an order magnitude higher than that of a-IGZO-TFTs (μ_{FE} ~7 $cm^2\ V^{-1}\ s^{-1}$). In contrast, Ochi *et al*.[7] reported that amorphous $IGZO_m$-TFTs showed a rather low μ_{FE} ~0.18 $cm^2\ V^{-1}\ s^{-1}$ for m ~14. Thus, the electron transport properties of $IGZO_m$-TFTs with higher m-values have yet to be clarified.

In 2001, Orita *et al*.[8] fabricated $IGZO_m$ films with a stable amorphous phase for $m < 4$. The Zn 4s orbitals predominantly contribute to the electron conduction of $IGZO_m$ with a large m-value. In 2006, Nomura *et al*.[9] precisely investigated the residual carrier concentration (n), which originated from oxygen deficiencies, and Hall mobility (μ_{Hall}) of the $IGZO_m$ system. They found that both n and μ_{Hall} increase as the m-value increases. Since the fabrication of TFTs with normally-off characteristics becomes difficult when n is high, reports on transistor characteristics of $IGZO_m$-TFTs with a large m-value are rare.[5, 7]

Here, we show that a Zn-rich composition enhances the electron transport properties of $IGZO_m$-TFTs. First, we clarified that the carrier effective mass (m^*) of $IGZO_m$ is independent of the m-value ($m^* = 0.16\ m_0$, m_0: electron mass). Then, we found that μ_{FE} of $IGZO_m$-TFT increased with the m-value for $m \leq 7$. This clearly reveals that the carrier relaxation time (τ) of $IGZO_m$ increases with m ($m \leq 7$). For $m > 7$, μ_{FE} decreases due to crystallization; The carrier electrons scatter at the grain boundaries. The best TFT performance occurs for $m = 7$ (μ_{FE} ~12 $cm^2\ V^{-1}\ s^{-1}$, subthreshold swing ~0.1 V $decade^{-1}$, and a negligibly small bias stress shift). We attempted thermopower (S) modulation analyses to clarify the electron transport properties of $IGZO_m$ and found that the effective channel thickness increased with m ($m \leq 7$). The present results provide an improving strategy towards new material design for next-generation TFTs with higher μ_{FE} values.

Experimental Section

Fabrication of $IGZO_m$ Films. $IGZO_m$ films (m = 1, 2, 3, 4, 5, 7, 9, 10, and 30) were deposited on alkali-free glass substrates (EAGLE XG®, Corning®) by a pulsed laser deposition (PLD) technique at room temperature. A KrF excimer laser (COMPex Pro 102, Coherent) was used to ablate the ceramic targets of $IGZO_m$. The laser fluence, repetition rate, and the number of pulses were ~2.3 J cm^{-2} $pulse^{-1}$, 10 Hz, and 1800 pulses, respectively. A constant oxygen pressure (1−5 Pa) was used during film deposition to control n. Afterwards, the films were annealed at several temperatures (50−150 °C) in air for 5 min to further control n.

Structure Analyses, Optical and Electron Transport Property Measurements of the IGZO$_m$ Films. The film thickness, relative density, and surface roughness of the resultant IGZO$_m$ films were measured by the X-ray reflectivity (XRR, Cu Kα_1, ATX-G, Rigaku). We also measured the X-ray diffraction (XRD) patterns of the resultant films. The incident angle of the X-ray was fixed at 0.5° while 2θ scanning was performed. The optical transmission and reflection spectra of the IGZO$_m$ films were recorded using a UV-Vis-NIR spectrophotometer (SolidSpec-3700, Shimadzu). We drew the absorption spectra (Tauc plot) and extracted the optical bandgap of the IGZO$_m$ films. The thermopower (S) was measured by a conventional steady-state method at room temperature. The Hall mobility (μ_{Hall}) and the volume carrier concentration ($n_{3\mathrm{D}}$) were measured by the dc four-probe method with a van der Pauw electrode configuration at room temperature, and ±7600 G was applied for the Hall effect measurements.

Fabrication of IGZO$_m$-TFTs. We fabricated IGZO$_m$-based TFTs (bottom-gate-top-contact type) on alkaline-free glass substrates (EAGLE XG®, Corning®). First, a 106-nm-thick AlO$_x$ film (dielectric permittivity ε_{r} = 8), which served as the gate insulator, was deposited by atomic layer deposition (ALD) onto an ITO-coated glass substrate. The capacitance (C_{i}) of the AlO$_x$ films was 67 nF cm^{-2}. Then ~20-nm-thick IGZO$_m$ film was deposited by PLD under an oxygen pressure of 5 Pa at room temperature through a stencil mask. The multilayer film was annealed at 350 °C in air for 5 min. Finally, 20-nm-thick Ti source/drain electrodes were evaporated through the stencil mask at room temperature.

Transistor Characterization and Electric Field Thermopower Modulation. Standard

transistor characteristics of the $IGZO_m$-TFTs were measured by a semiconductor device analyzer (B1500A, Agilent) at room temperature. We calculated the field effect mobility (μ_{FE}) by using following equation (1),

$$\mu_{FE} = \frac{g_m}{C_i \frac{W}{L} V_D} \qquad (1)$$

where g_m is the transconductance, C_i is the capacitance per unit area of the gate insulator (67 nF cm^{-2} for AlO_x), W is the channel width, L is the channel length, and V_D is the drain voltage. We obtained μ_{FE} using the maximum value of g_m. Thermopower modulation analyses of the $IGZO_m$-TFTs were performed at room temperature in air. Details of the thermopower modulation analyses are published elsewhere ($SrTiO_3$-TFTs,[10] $InGaZnO_4$-TFTs,[11] $BaSnO_3$-TFTs,[12] SnO_2-TFTs,[13] $InSnZnO_x$-TFTs,[14] and GaN-TFTs[15]).

Results and Discussion

First, we fabricated $IGZO_m$ films and analyzed their structure and optical properties. **Figure 1a** shows the XRD patterns of the resultant $IGZO_m$ films. For $m \leq 7$, a halo of $IGZO_m$ appears at 2θ ~34°, whereas sharp diffraction peaks appear for $m > 7$. These results indicate that films with $m \leq 7$ are amorphous whereas those with $m > 7$ are randomly-oriented polycrystalline. These observations are consistent with the report by Orita *et al*. in which $IGZO_m$ crystallized at room temperature for $m > 5$.[8] The optical bandgap (**Figure 1b**) gradually decreases as the m-value increases (3.25 eV for $m = 1$ and 3.15 eV for $m = 5$). This tendency is similar to that of polycrystalline $IGZO_m$.[16] These observations demonstrate that $IGZO_m$ (m = 1, 2, 3, 4, 5, 7, 9, and 30) films are successfully fabricated.

Then, we measured the electron transport properties of the $IGZO_m$ films. **Figure 2a** plots the thermopower (S) as a function of the volume carrier concentration (n_{3D}) for the resultant $IGZO_m$ films at room temperature in air. The S-values are always negative, confirming that the films are n-type semiconductors. The absolute value of S decreases with n_{3D} in all cases. The density of states effective mass (m^*) was extracted using the relationship between n_{3D} and S.[17] Although the data is a bit scattered due to the difficulty of accurate n_{3D} measurement when the mobility is small, all the S–n_{3D} relationships follow a simulated line with a carrier effective mass (m^*) of 0.16 m_0, similar to the reported m^* of a-IGZO ($m_d^*/2 = 0.17\ m_0$)[18-20], indicating that m^* does not depend on the m-values (Note we extracted averaged value since the data was scattered, though extraction of m^* requires accurate carrier concentration values). This indicates that the Zn 4s orbital dominated conduction band bottom exhibits a similar band dispersion to that of the In 5s orbital dominated conduction band bottom. In contrast, μ_{Hall} does not show a clear trend as a function of n_{3D} (**Figure 2b**). Since all $IGZO_m$ films have similar m^* values, the difference in the observed μ_{Hall} is due to the variation in the carrier relaxation time ($\tau = e\cdot(\mu\cdot m^*)^{-1}$). Since the $IGZO_m$ films were deposited with different oxygen pressure as well as with different annealing temperatures in order to tune the carrier concentration, the film quality of the $IGZO_m$ films were different each other. The difference in the film quality largely affects carrier relaxation time. Therefore, the Hall effect measurement was a bit difficult when the film quality was poor.

Next, we fabricated $IGZO_m$-TFTs on ITO-AlO_x glass-insulator substrates and measured their transistor characteristics. Compared to the other high-k dielectrics, AlO_x has a

relatively larger band offset with $IGZO_m$.[21, 22] Therefore, we expected that the gate leakage current and bias instabilities would be suppressed by the use of AlO_x gate insulator for $IGZO_m$-TFTs. **Figure 3a** shows the typical transfer characteristics of $IGZO_m$-TFTs at room temperature. The channel length (L), width (W), and applied drain voltage (V_d) are 100 μm, 400 μm, and +5 V in all cases, respectively. The on current gradually increases with m for $m \leq 7$. However, the off current increases and the on current gradually decreases with m for $m > 7$. **Figure 3b** plots μ_{FE} of the $IGZO_m$-TFTs. For $m \leq 7$, μ_{FE} gradually increases with m, but it decreases with m for $m > 7$. The highest μ_{FE} is ~12 $cm^2\ V^{-1}\ s^{-1}$ for $m = 7$. It is noteworthy that the low μ_{FE} values of m = 10 and 30 should originate from the grain boundaries since $IGZO_m$ crystallizes for $m >$ 7. This is also reflected by the subthreshold swing (*S.S.*) value. The *S.S.* value remains almost constant (~0.1 V $decade^{-1}$) for m = 1– 7 but it increases from 0.1–0.3 V $decade^{-1}$ for higher values of m. This would be attributed to the increase in oxygen deficiency-related defects at the interface of the $IGZO_m$ channel layer and the gate dielectric.

To clarify the origin of why m = 7 TFT exhibited the highest μ_{FE}, various gate voltages were applied to measure the thermopower of the $IGZO_m$-TFTs (**Figure 4a**, electric field thermopower modulation analyses). A constant V_g was initially applied to the TFTs to accumulate carrier electrons. Then, S of the channel was measured during the V_g application. **Figure 4b** plots the electric field modulated S as a function of n_{2D}. For m = 1 and 2, several S-values around the lower n_{2D} are not on a straight line, which may be due to the non-parabolic shaped tail states[23] just below the original conduction band bottom at a lower m-value.[11] It shows a decreasing tendency when n_{2D} is high. On the other hand, the absolute values of S for m = 3, 5, and 7 showed a simple decreasing

tendency. It should be noted that $|S|$ increases as the m-value increases. Then, we compared the n_{2D} (**Figure 4b**) with n_{3D} (**Figure 2a**) for a given $|S|$ (**Figure 4b**) to estimate the effective channel thickness (n_{2D}/n_{3D}). Interestingly, the n_{2D}/n_{3D} increases from ~5 nm to ~28 nm with m-value, similar to the increasing tendency of μ_{FE}. Thus, an increase of τ with m-value originates from the increase of the effective channel thickness. An increased thickness reduces electron scattering at the interface between dielectric and semiconducting channel. It should be noted that the field effect mobility is obtained with the Fermi energy level above the conduction band edge, at carrier scattering at defect centers becomes negligibly small.

According to the Poisson equation, the carrier accumulation layer becomes thick when the dielectric permittivity of the semiconductor is large or the residual carrier concentration is high. The dielectric constant of amorphous $InGaZnO_4$ is 16[24] and that of ZnO is ~9[25]. Therefore, it is impossible to explain the origin of why the effective thickness of $IGZO_m$ increases with m using the dielectric constant scenario. In short, the thickness increase with m is most likely due to an increase of the residual carrier concentration with m. Since the bandgap of $IGZO_m$ decreased with m, the increasing tendency of the residual carrier concentration with m is reasonable.

Finally, we performed the positive bias stress (PBS) and negative bias stress (NBS) measurements for TFTs with $m \leq 7$. For NBS, TFTs were evaluated in ambient air at V_g = −20 V for a total stress time of 10000 s. Except for m = 1, the transfer characteristics of the TFTs do not change significantly after NBS (**Figures S1b−S4b)**. In contrast, for PBS with V_g = +20 V, the stress conditions affect the positive ΔV_{th} **(Figures S1a−S4a**).

This would be attributed to charge trapping in gate insulators and the creation of electron traps in the channel. **Figure S5** shows the change in the normalized V_{th} shift of the IGZO$_m$-TFTs under both PBS and NBS as a function of the stress time. Large V_{th} shift occurs after PBS for m = 1 **(Figure S1a)**, indicating that n_{2D} should be lower than that assumed as $C_i \cdot (V_g - V_{th})$. In contrast, the V_{th} shift for m = 3, 5, and 7 (**Figures S2a, S3a, and S4a**) is negligible, indicating that the electric field thermopower measurements provide an accurate and effective channel thickness. These results reveal that m = 7 IGZO$_m$-TFT exhibits the best TFT characteristics (μ_{FE} ~12 cm^2 V^{-1} s^{-1}, *S.S.* ~0.1 V decade^{-1} and a negligibly small bias stress shift) because the wider effective channel thickness provides a longer τ. The present results provide an improving strategy towards new material design for next-generation TFTs with higher μ_{FE} values.

Conclusion

We studied the electron transport properties of InGaO$_3$(ZnO)$_m$ (m = 1−30) with higher m-values (IGZO$_m$) thin films and TFTs. The best TFT performance was obtained for m = 7 (μ_{FE} ~12 cm^2 V^{-1} s^{-1}, subthreshold swing ~0.1 V decade^{-1}, and a negligibly small bias stress shift). First, we clarified that the m* of IGZO$_m$ films is 0.16 m_0, independent of the m-value. Then, we found that μ_{FE} of IGZO$_m$-TFT increased with the m-value for $m \leq$ 7, whereas it decreased for m >7 due to the crystallization. The thermopower modulation analyses revealed that the effective channel thickness increased with m ($m \leq$ 7) that resulted in the longer τ. The present results provide an improving strategy towards new material design for next-generation TFTs with higher μ_{FE} values.

ASSOCIATED CONTENT

The Supporting Information is available free of charge at https://pubs.acs.org/doi/10.1021/acs.jpcc.xxxxxxx.

Bias stress characteristics of $IGZO_1$-TFT, Bias stress characteristics of $IGZO_3$-TFT, Bias stress characteristics of $IGZO_5$-TFT, Bias stress characteristics of $IGZO_7$-TFT, Normalized V_{th} shift (ΔV) as a function of stress time.

Author Information

Corresponding Authors

Prashat Ghediya − Research Institute for Electronic Science, Hokkaido University, N20W10, Kita, Sapporo 001-0020, Japan

ORCiD: orcid.org/ 0000-0001-9953-0471

Email: prashantghediya@gmail.com

Hiromichi Ohta − Research Institute for Electronic Science, Hokkaido University, N20W10, Kita, Sapporo 001-0020, Japan

ORCiD: orcid.org/0000-0001-7013-0343

Email: hiromichi.ohta@es.hokudai.ac.jp

Authors

Hui Yang − Research Institute for Electronic Science, Hokkaido University, N20W10, Kita, Sapporo 001-0020, Japan; Institute of Optoelectronic Technology, Beijing Jiaotong University, Beijing 100044, China

ORCiD: orcid.org/ 0000-0002-2287-2243

Takashi Fujimoto − Graduate School of Information Science and Technology, Hokkaido University, Sapporo 060-0814, Japan

Yuqiao Zhang − Institute of Quantum and Sustainable Technology, Jiangsu University, Zhenjiang 212013, China; Foshan (Southern China) Institute for New Materials, Foshan 528200, China
ORCiD: orcid.org/0000-0001-7579-4923

Yasutaka Matsuo − Research Institute for Electronic Science, Hokkaido University, N20W10, Kita, Sapporo 001-0020, Japan
ORCiD: orcid.org/0000-0002-5071-0284

Yusaku Magari − Research Institute for Electronic Science, Hokkaido University, N20W10, Kita, Sapporo 001-0020, Japan
ORCiD: orcid.org/0000-0001-9655-4283

Author Contributions

P.G., H.Y., T.F., and H.O. fabricated the samples and measured the transistor characteristics and thermopower. Y.Z. analyzed the thermopower. Y. Matsuo fabricated the AlO_x films. Y. Magari analyzed the transistor characteristics. H.O. planned and supervised the project. All authors discussed the results and commented on the manuscript.

Funding

H.Y. received a scholarship from the China Scholarship Council (202107090085). Y. Magari received funding from a Grant-in-Aid of the JSPS (22K14303). H.O. received funding from Grants-in-Aid of the JSPS (19H05788, 22H00253). Y.Z. received funding from the Start-Up Fund of Jiangsu University (5501310015), Guangdong Basic and Applied Basic Research Foundation (2021A1515110881), and the Youth Fund of Foshan (Southern China) Institute for New Materials (2021AYF25009).

Notes

The authors declare no competing financial interest.

Acknowledgements

Part of this work was supported by "Advanced Research Infrastructure for Materials and Nanotechnology in Japan (ARIM)" of the Ministry of Education, Culture, Sports, Science and Technology (MEXT), the Crossover Alliance to Create a Future with People, Intelligence and Materials, and the Network Joint Research Center for Materials and Devices.

References

(1) Hosono, H.; Kumomi, H., *Amorphous oxide semiconductors : IGZO and related materials for display and memory*. Wiley: Hoboken, NJ, 2022; p pages cm.

(2) Hosono, H. How We Made the IGZO Transistor. *Nat. Electron.* **2018,** 1, 428-428.

(3) Nomura, K.; Ohta, H.; Takagi, A.; Kamiya, T.; Hirano, M.; Hosono, H. Room-temperature Fabrication of Transparent Flexible Thin-film Transistors using Amorphous Oxide Semiconductors. *Nature* **2004,** 432, 488-492.

(4) Kimizuka, N.; Isobe, M.; Nakamura, M. Syntheses and Single-Crystal Data of

Homologous Compounds, $In_2O_3(ZnO)_m$ (m = 3, 4, and 5), $InGaO_3(ZnO)_3$, and $Ga_2O_3(ZnO)_m$ (m = 7, 8, 9, and 16) in the In_2O_3-$ZnGa_2O_4$-ZnO System. *J. Solid State Chem.* **1995,** 116, 170-178.

(5) Nomura, K.; Ohta, H.; Ueda, K.; Kamiya, T.; Hirano, M.; Hosono, H. Thin-film transistor fabricated in single-crystalline transparent oxide semiconductor. *Science* **2003,** 300, 1269-1272.

(6) Ohta, H.; Nomura, K.; Orita, M.; Hirano, M.; Ueda, K.; Suzuki, T.; Ikuhara, Y.; Hosono, H. Single-crystalline films of the homologous series $InGaO_3(ZnO)_m$ grown by reactive solid-phase epitaxy. *Adv. Funct. Mater.* **2003,** 13, 139-144.

(7) Ochi, M.; Hino, A.; Goto, H.; Hayashi, K.; Kugimiya, T. Electrical Characterization of Zinc-Rich Amorphous In-Ga-Zn-O Thin Film Transistors. *Phys. Status Solidi A* **2018,** 215, 1800085.

(8) Orita, M.; Ohta, H.; Hirano, M.; Narushima, S.; Hosono, H. Amorphous transparent conductive oxide $InGaO_3(ZnO)_m$ ($m \leq 4$): a Zn 4s conductor. *Philo. Mag. B* **2001,** 81, 501-515.

(9) Nomura, K.; Takagi, A.; Kamiya, T.; Ohta, H.; Hirano, M.; Hosono, H. Amorphous Oxide Semiconductors for High-performance Flexible Thin-film Transistors. *Jpn. J. Appl. Phys.* **2006,** 45, 4303-4308.

(10) Ohta, H.; Masuoka, Y.; Asahi, R.; Kato, T.; Hosono, H. Field-modulated thermopower in $SrTiO_3$-based field-effect transistors with amorphous $12CaO7Al_2O_3$ glass gate insulator. *Appl. Phys. Lett.* **2009,** 95, 703.

(11) Koide, H.; Nagao, Y.; Koumoto, K.; Takasaki, Y.; Umemura, T.; Kato, T.; Ikuhara, Y.; Ohta, H. Electric Field Modulation of Thermopower for Transparent Amorphous Oxide Thin Film Transistors. *Appl. Phys. Lett.* **2010,** 97, 182105.

(12) Sanchela, A. V.; Wei, M.; Cho, H. J.; Ohta, H. Thermopower Modulation Clarification of the Operating Mechanism in Wide Bandgap $BaSnO_3$-$SrSnO_3$ Solid-Solution Based Thin Film Transistors. *Small* **2019,** 15, 1805394.

(13) Liang, D. D.; Zhang, Y. Q.; Hai, J. C.; Ohta, H. Electric field thermopower modulation analyses of the operation mechanism of transparent amorphous SnO_2 thin-film transistor. *Appl. Phys. Lett.* **2020,** 116, 143503.

(14) Yang, H.; Zhang, Y.; Matsuo, Y.; Magari, Y.; Ohta, H. Thermopower Modulation Analyses of High-Mobility Transparent Amorphous Oxide Semiconductor Thin-Film Transistors. *ACS Appl. Electron. Mater.* **2022**.

(15) Ohta, H.; Kim, S. W.; Kaneki, S.; Yamamoto, A.; Hashizume, T. High Thermoelectric Power Factor of High-mobility 2D Electron Gas. *Adv. Sci.* **2018,** 5, 201700696.

(16) Préaud, S.; Byl, C.; Brisset, F.; Berardan, D. SPS-assisted synthesis of $InGaO_3(ZnO)_m$ ceramics, and influence of *m* on the band gap and the thermal conductivity. *J. Am. Ceram. Soc.* **2020,** 103, 3030-3038.

(17) Vining, C. B. A model for the high-temperature transport properties of heavily doped n-type silicon-germanium alloys. *J. Appl. Phys.* **1991,** 69, 331-341.

(18) Takagi, A.; Nomura, K.; Ohta, H.; Yanagi, H.; Kamiya, T.; Hirano, M.; Hosono, H. Carrier transport and electronic structure in amorphous oxide semiconductor, a-$InGaZnO_4$. *Thin Solid Films* **2005,** 486, 38-41.

(19) Nomura, K.; Kamiya, T.; Ohta, H.; Uruga, T.; Hirano, M.; Hosono, H. Local coordination structure and electronic structure of the large electron mobility amorphous oxide semiconductor In-Ga-Zn-O: Experiment and ab initio calculations. *Phys. Rev. B* **2007,** 75, 035212.

(20) Kamiya, T.; Nomura, K.; Hosono, H. Present status of amorphous In-Ga-Zn-O thin-

film transistors. *Sci. Technol. Adv. Mater.* **2010,** 11, 044305.

(21) Mukherjee, A.; Ottapilakkal, V.; Sagar, S.; Das, B. C. Ultralow-Voltage Field-Effect Transistors Using Nanometer-Thick Transparent Amorphous Indium–Gallium − Zinc Oxide Films. *ACS Appl. Nano Mater.* **2021,** 4, 8050-8058.

(22) Kang, I. H.; Hwang, S. H.; Baek, Y. J.; Kim, S. G.; Han, Y. L.; Kang, M. S.; Woo, J. G.; Lee, J. M.; Yu, E. S.; Bae, B. S. Interfacial Oxidized Gate Insulators for Low-Power Oxide Thin-Film Transistors. *ACS Omega* **2021,** 6, 2717-2726.

(23) Ide, K.; Nomura, K.; Hosono, H.; Kamiya, T. Electronic Defects in Amorphous Oxide Semiconductors: A Review. *Phys. Status Solidi A* **2019,** 216, 1800372.

(24) Zhang, J. W.; Li, Y. P.; Zhang, B. L.; Wang, H. B.; Xin, Q.; Song, A. M. Flexible indium-gallium-zinc-oxide Schottky diode operating beyond 2.45 GHz. *Nat Commun* **2015,** 6, 7561.

(25) Vegesna, S. V.; Bhat, V. J.; Burger, D.; Dellith, J.; Skorupa, I.; Schmidt, O. G.; Schmidt, H. Increased static dielectric constant in ZnMnO and ZnCoO thin films with bound magnetic polarons. *Scientific Reports* **2020,** 10, 6698.

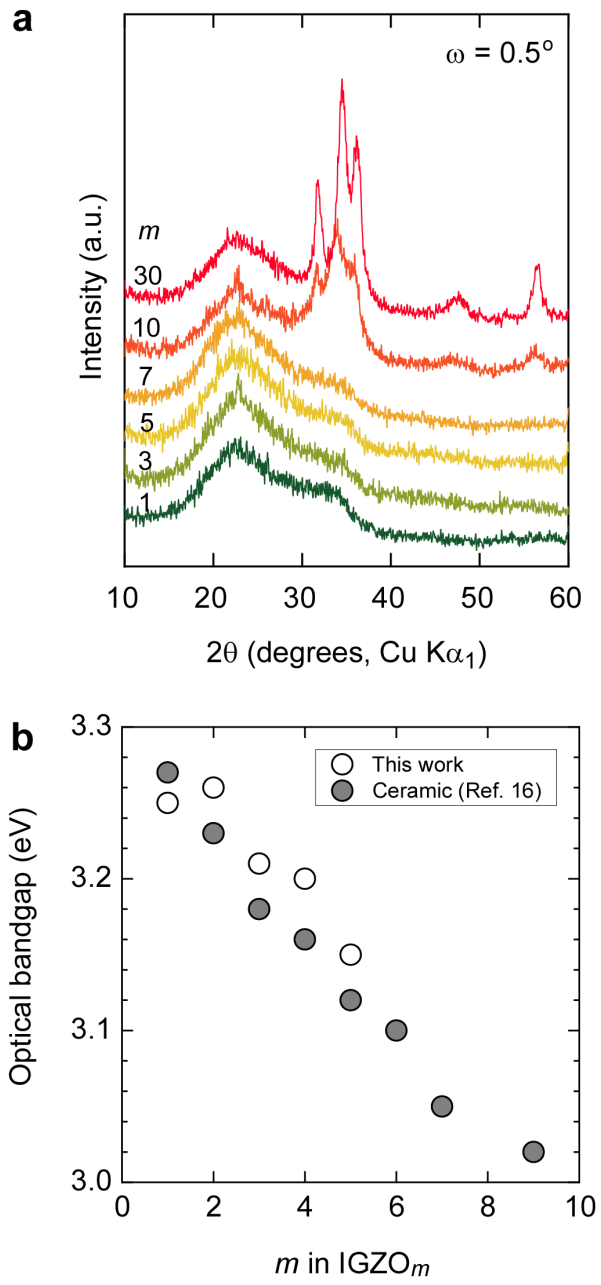

Figure 1. Structural and optical characterization of the resultant IGZO$_m$ films. (a) XRD patterns with a fixed X-ray incident angle of 0.5°. For $m \leq 7$, a halo of IGZO$_m$ is seen at 2θ ~34°, whereas sharp diffraction peaks appear for $m > 7$. For $m > 7$, crystallization occurs. (b) Optical bandgap. As m increases, the optical bandgap of IGZO$_m$ decreases, which is a similar overall tendency as that of IGZO$_m$ ceramics.[16]

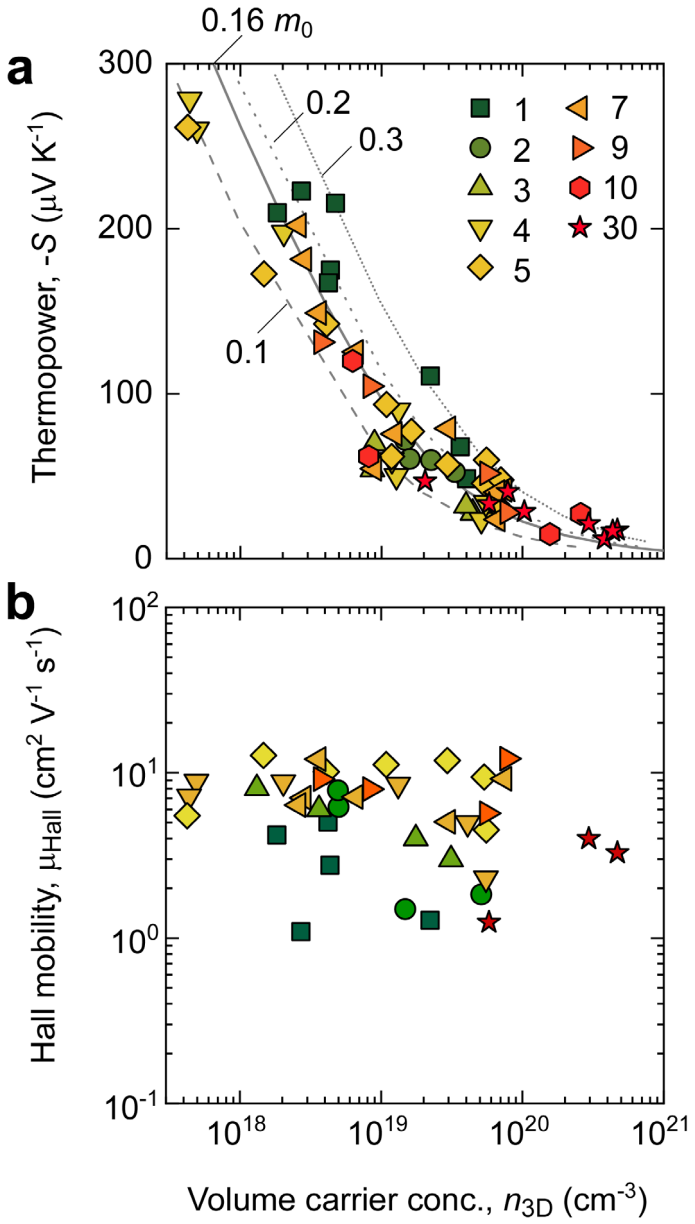

Figure 2. Electron transport properties of the a-IGZO$_m$ films at room temperature. Changes in (a) thermopower (S) and (b) Hall mobility (μ_{Hall}) with the volume carrier concentration (n_{3D}). (a) shows a clear trend, but (b) does not.

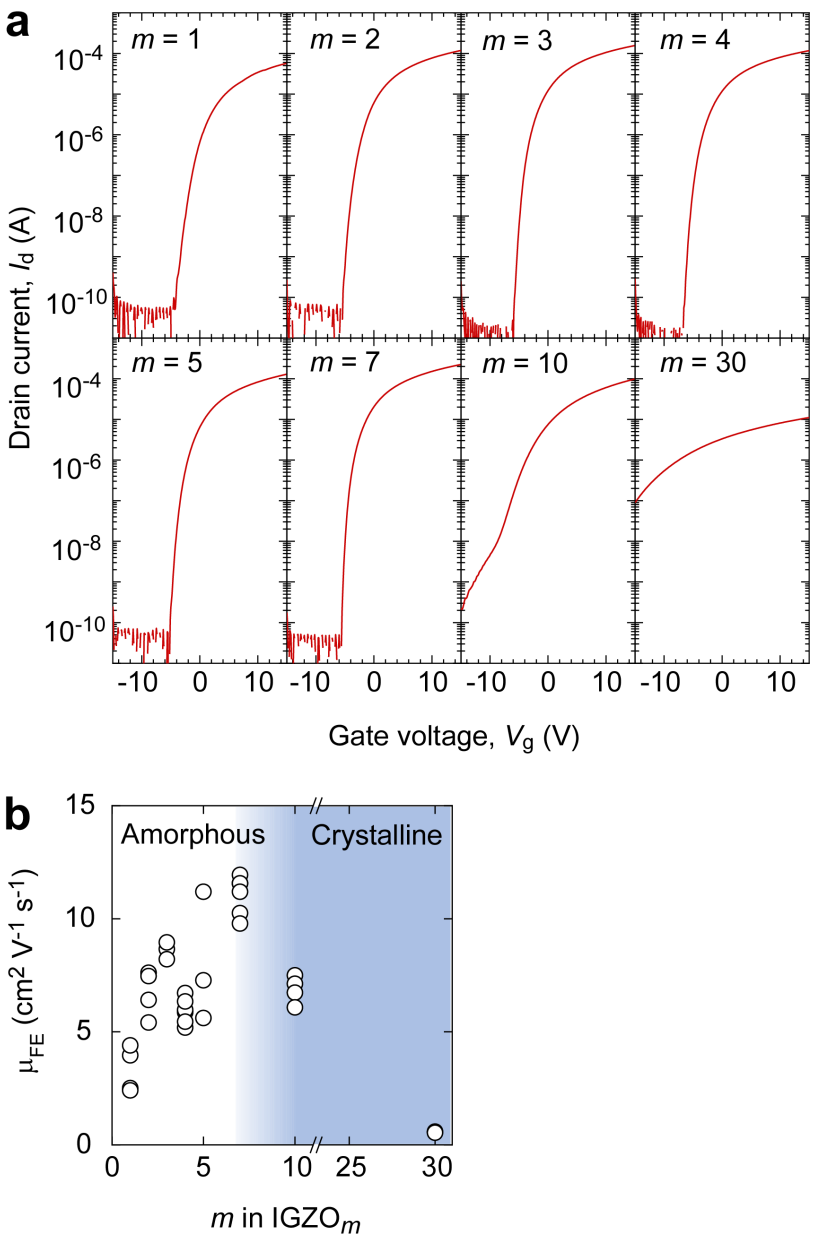

Figure 3. Typical transistor characteristics of IGZO$_m$-TFTs at room temperature. (a) Transfer characteristics (L = 100 μm, W = 400 μm, V_d = +5 V). On current gradually increases with m for $m \leq 7$. For $m > 7$, the off current increases and the on current gradually decreases with m. (b) Field effect mobility of the IGZO$_m$-TFTs. For $m \leq 7$, μ_{FE} gradually increases with m, but it drops with m for $m > 7$. Highest μ_{FE} is ~12 cm^2 V^{-1} s^{-1}, which is obtained for m = 7.

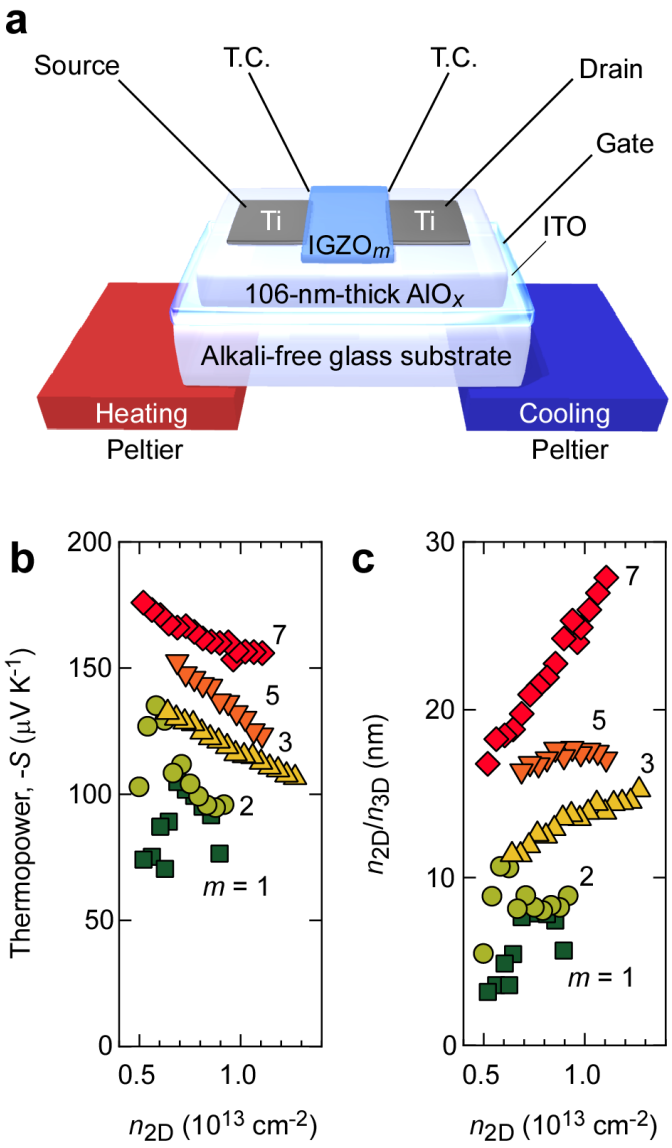

Figure 4. Electric field thermopower modulation analyses of the IGZO$_m$-TFTs. (a) Schematic of the experimental setup. IGZO$_m$-TFT is placed between two Peltier devices. Upon applying a gate voltage, the thermopower is measured by applying a temperature difference between the source and drain electrodes. (b) Thermopower and (c) effective thickness of IGZO$_m$-TFTs as a function of n_{2D}. Note that the effective thickness (n_{2D}/n_{3D}) varies from ~2 nm to ~28 nm depending on the m-value.